Numerical simulations of quantum transport in semiconductor nanowires

Oscar Erlandsson

Bachelor's thesis
January, 2016

LUND UNIVERSITY
Faculty of Science

Project duration: 2 months

Department of Physics
Division of Mathematical Physics

Supervised by: Peter Samuelsson

Abstract

The study of electronic transport in chemically synthesized semiconductor nanowires is an active field of research, with potential applications in areas such as quantum computing and nanoelectronics. Motivated by recent experimental progress, we use a simple non-atomistic tight-binding model implemented in open-source software to simulate quantum electronic transport in such nanowires. Including various physical effects (such as those arising from finite temperature and a uniform magnetic field) we present a ‘‘toolset’’ for computing their scattering matrix in general and conductance in particular.

List of abbreviations

The following abbreviations are used in the text

- 2DEG Two-dimensional electron gas
- GDM Gaussian Disorder Model

Table of contents

Section 1
Introduction

The fabrication, characterization and applications of nanowires are integral parts of modern nanotechnology. Having dimensions in the nanoscale regime, nanowires have been constructed in various shapes and sizes, using both metallic and semiconductor materials. The latter type, semiconductor nanowires, have several unique features, such as high suitability to be incorporated in nanoelectronic devices like transistors. As presented in Ref. [1], a great amount of experimental progress has been made since the inception of the field. Areas in which semiconductor nanowires have potential technical applications include photovoltaics, quantum computing and nanoelectronics. Hence, advancement of the understanding of these devices contributes to the technological development and have the potential of unlocking new ways for society to improve its energy efficiency. An overview of the relevant experimental background is presented in Section 3.

For several aspects of the characterization and application of semiconductor nanowires their electronic transport properties are important. A theoretical framework suitable for describing these properties at the nanoscale is known as ''conductance from transmission'', and was developed largely by R. Landauer in the 20th century [2, 3]. One of its landmark experimental signatures, conductance quantization, was observed for the first time in the 1980s. We present the transmission approach and related experimental results in Sections 2 and 3, respectively.

In this project, we simulate electronic transport in semiconductor nanowires based on the transmission approach, using a tight-binding model implemented in the recently developed open-source software package Kwant [4]. The aim of the project is to provide a numerical toolset for predicting the electronic transport behavior in a typical semiconductor nanowire experiment, by including models of relevant physical effects in the simulations. The qualitative results of the simulations, and the possibility of easily implementing a specific experimental setup, may enable a better understanding of the electronic transport and aid the experimental process in general.

More specifically, we are using a conduction-band, non-atomistic tight-binding model. This model comes with a number of limitations. Perhaps most notably, it does not discriminate between crystal structures, and material properties are effectively only implemented by the effective mass appearing in an energy unit prefactor. This property of the model could, however, also be seen as a strength in that it offers a great simplicity. In summary, the model enables us to include phenomena which are strictly quantum within a relatively compact framework. This can be put in contrast to other approaches to calculating transport properties, such as using the ab initio Density Functional Theory. Such an approach will provide a more complete picture, but could also be more complicated to implement for different experimental setups.

Section 2

Quantum transport of electrons: Theory and formalism

The approach of conductance from transmission was pioneered by R. Landauer [2, 3] and has since been used and expanded upon by many others. In particular, M. Büttiker extended the framework to include multi-terminal systems [5], resulting in the Landauer-Büttiker formalism. Based on the presentation of the theory in Ref. [6] (its Section 2.1, 2.2, 2.5 and 3.1) we here derive the Landauer formula of conductance, connect it to the scattering matrix and discuss some further properties of this matrix.

2.1 Landauer formula of conductance

In order to study the properties of quantum electronic transport we derive an expression for the electric conductance G of a scattering conductor with the average probability $\tilde{T}(E)$ for an electron to transmit across it. We consider the system as illustrated in Figure 1. In this discussion we will consider a two-dimensional system, but we will arrive at general results which can be used in three dimensions as well. The important point is that one dimension is the propagating one, the axis of which is connecting the leads and the remaining dimensions are transversal. The conductor is fixed between two leads labeled 1 and 2 at chemical potentials μ_1 and μ_2. We assume that electrons in Lead i are distributed according to a Fermi function

$$f_i(E) = \frac{1}{\exp(\frac{E-\mu_i}{k_B T}) + 1} \tag{1}$$

where k_B is the Boltzmann constant, T is temperature and E is energy. The leads are fully ballistic and are similar to the conductor in one end and in contact with large electron reservoirs in the other. These reservoirs are assumed to be large enough for electrons to be able to enter them with zero probability of reflection.

For a given finite energy E, electrons occupy $\pm k$-states in a finite number $N(E)$ of transverse modes (which we, for simplicity, assume to be the same in both leads), where k is the wave vector in the propagating direction; $+k$-states carry positive current and vice versa. In general the dispersion relations $E(k)$ and hence $N(E)$ depend on the transversal geometry and confinement, and we make no particular choice here.

Consider the cloud of $+k$-electrons in Lead 1 corresponding to a single transversal mode, the individual states of which being occupied according to the Fermi function $f_1(E)$. The cloud is moving with a group velocity v_g in the positive propagating direction. The

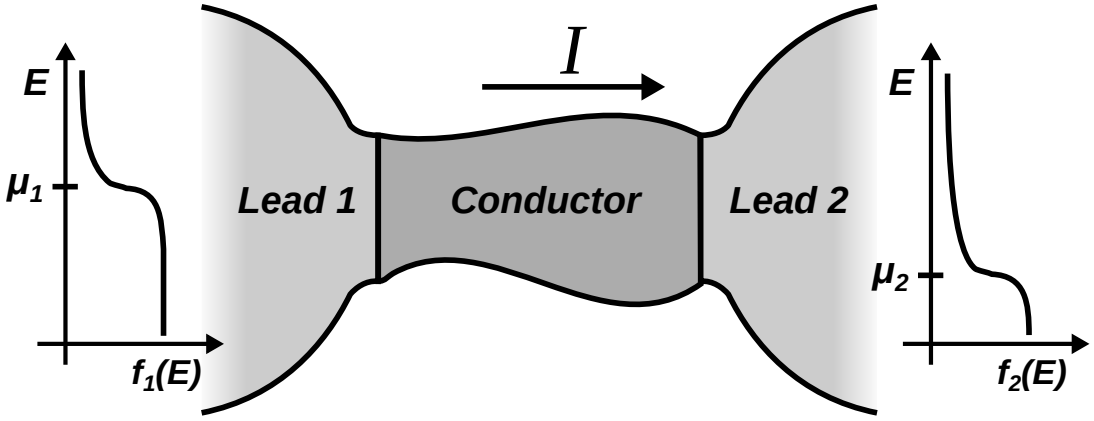

Figure 1: *A conductor placed between two leads at chemical potentials μ_1 and μ_2. The Fermi functions f_1 and f_2 describe the occupancy of states in the leads.*

current $\tilde{I}^1_{k>0}$ carried by these electrons is given by

$$\tilde{I}^1_{k>0} = \sum_{k>0} env_g f_1(E) = \frac{en}{\hbar} \sum_{k>0} \frac{\partial E}{\partial k} f_1(E) \tag{2}$$

where e is the elementary charge, n is the electron density in the propagating dimension, $\hbar$ is Planck's constant h divided by 2π and we have used the relation for propagating waves that

$$v_g = \frac{\partial \omega}{\partial k} = \frac{1}{\hbar} \frac{\partial E}{\partial k} \tag{3}$$

where ω is the angular frequency. Assuming periodic boundary conditions in the propagating dimension, the sum can be written as an integral by considering the k-space geometry

$$\tilde{I}^1_{k>0} = \frac{en}{\hbar} \frac{2}{2\pi n} \int_0^{+\infty} \frac{\partial E}{\partial k} f_1(E)\, \mathrm{d}k = \frac{2e}{h} \int_{E_0}^{+\infty} f_1(E)\, \mathrm{d}E \tag{4}$$

where E_0 is the band bottom (the minimum energy for $k > 0$) and we have assumed that two electrons can occupy each state due to spin degeneracy. This result can then be generalized to the current $I^1_{k>0}$ carried by $+k$-electrons of all occupied transversal modes

$$I^1_{k>0} = \frac{2e}{h} \int_{-\infty}^{+\infty} f_1(E) N(E)\, \mathrm{d}E \ . \tag{5}$$

The flux of electrons $i_1^{\rightarrow}$ (current per energy), in Lead 1 moving into the conductor is then given by

$$i_1^{\rightarrow} = \frac{2e}{h} f_1(E) N(E) \ . \tag{6}$$

Similarly, for the flux of electrons in Lead 2 moving into the conductor

$$i_2^{\leftarrow} = \frac{2e}{h} f_2(E) N(E) \ . \tag{7}$$

There is no contribution from reflected electrons since we have assumed that electrons enter the reservoirs without reflection, meaning e.g. that once $+k$-electrons enter Lead 2 they will ''disappear'' into the reservoir it is attached to. The flux $i_1^{\leftarrow}$ of electrons in Lead 1 moving away from the conductor is the sum of the reflected part of $i_1^{\rightarrow}$ and the transmitted part of $i_2^{\leftarrow}$,

$$i_1^{\leftarrow} = \left(1 - \tilde{T}(E)\right) i_1^{\rightarrow} + \tilde{T}(E) i_2^{\leftarrow} \ , \tag{8}$$

and since the total electron flux i_e is the same everywhere, we can calculate it in Lead 1,

$$i_e = i_1^{\rightarrow} - i_1^{\leftarrow} = \frac{2e}{h} N(E) \tilde{T}(E) \left(f_1(E) - f_2(E)\right) \ . \tag{9}$$

We integrate this expression to obtain the electric current, defining the total transmission probability $T(E) = N(E)\tilde{T}(E)$,

$$I = \frac{2e}{h} \int_{-\infty}^{+\infty} T(E) \left(f_1(E) - f_2(E)\right) \mathrm{d}E \tag{10}$$

With the current I written on this form, there are several ways to define the conductance G. In this text we will work with two definitions, both on the basic form

$$G = \frac{I}{V_{SD}} \tag{11}$$

where V_{SD} is the applied bias $V_{SD} = (\mu_1 - \mu_2)/e$. From this expression, we first formulate a formula for the linear response conductance G_{LR}, for $V_{SD} \to 0$. In this limit, we obtain the expression

$$G_{\mathrm{LR}}(E_F) = \frac{2e^2}{h} \int_{-\infty}^{+\infty} T(E) f_t \, \mathrm{d}E \tag{12}$$

where E_F is the Fermi energy and f_t is the thermal broadening function, given by

$$f_t = -\frac{\partial}{\partial E} \left(\frac{1}{\exp(\frac{E - E_F}{k_B T}) + 1} \right) \ . \tag{13}$$

For sufficiently large V_{SD} the linear response result is inadequate and a potential distribution arises inside of the conductor, in principle modifying the transmission probability $T(E)$. For simplicity, however, we assume that the voltage drop occurs entirely in the contacts, so that $T(E)$ is unchanged. More details on the justification of this assumption is provided in Ref. [6]. With this assumption, we can write

$$\mu_1 = E_F + \frac{eV_{SD}}{2} \qquad \text{and} \qquad \mu_2 = E_F - \frac{eV_{SD}}{2} \tag{14}$$

for voltage drops occurring symmetrically in the contacts. From the expression in (11) we then obtain

$$G(E_F, V_{SD}) = \frac{2e^2}{h} \frac{1}{V_{SD}} \int_{-\infty}^{+\infty} T(E) \left(f_1(E) - f_2(E)\right) \mathrm{d}E \tag{15}$$

which is our full expression for the bias-dependent conductance. We note that the prefactors (as functions of energy) to the total transmission probability $T(E)$ in equations (12) and (15) represent very sharp peaks around E_F as the temperature T, as well as the applied bias V_{SD} in the non-linear response case, approach zero. Hence, since $N(E)$ increases in discrete steps as new transverse modes become available, these equations imply that the increase of conductance occurs in quanta of $G_0 = 2e^2/h$ for transport in the near-ballistic regime with low temperature and low applied bias. Finally, we note that in the remainder of this text, the symbol E will denote the Fermi energy instead of the integration variable in the above equations.

2.2 The scattering matrix

The effective mass Schrödinger equation for an electron in either of the leads in the setup illustrated in Figure 1, with an applied magnetic field, is given by $H\Psi = E\Psi$ with the Hamiltonian

$$H = \frac{(p - eA)^2}{2m^*} + V \tag{16}$$

where p is momentum, m^* the electron effective mass, A the vector potential and V the scalar potential. The vector potential A depends on the configuration of the magnetic field and the electrostatic potential V depends on the geometry and confinement of the system and other applied potentials that might be included in the model.

We will carry out no explicit analytical solution of the Schrödinger equation in this text, but we note that it is in principle possible to solve it in many cases, at least numerically. For simplicity, we here assume both leads to have the same number N of occupied transversal modes at some particular energy. Then, once full solutions corresponding to all these modes are obtained the scattering matrix, or S-matrix, can be written down, as given by

$$c_{\text{out}} = S c_{\text{in}} \tag{17}$$

where c_{out} (c_{in}) is the column vector of the outgoing (incoming) complex wave amplitudes and S is the $2N \times 2N$ scattering matrix connecting them. In this formulation, the S-matrix consists of four sub-matrices

$$S = \begin{pmatrix} r & t' \\ t & r' \end{pmatrix} \tag{18}$$

where t and r are transmission and reflection amplitude matrices for electrons originating in the reservoir connected to Lead 1, and t', r' are the corresponding quantities for the reservoir connected to Lead 2. The total transmission probability $T(E)$, is then given by

$$T(E) = \sum_{i,j} |t_{ij}|^2 = \text{tr}(tt^\dagger) \ . \tag{19}$$

We make some additional remarks. First, we note that S has the property of unitarity due to current conservation. Second, we note that even though we relate it exclusively to conductance in this project, the S-matrix of a system provides quite a general description

of its transport properties; for example, thermoelectric coefficients and (thermal and shot) noise can be expressed in terms of scattering matrix elements, as described e.g. in Refs. [7] and [8], respectively.

Section 3

Experimental background

The most significant condition for quantized conductance to occur is that the dimensions of the system should be comparable to its Fermi wavelength λ_F. Here, the Fermi wavelength of a material means the de Broglie wavelength of electrons at the Fermi energy in the material. A short summary of relevant experiments where this condition has been fulfilled and conductance quantization has been observed is presented below. We then describe some details of a typical electronic transport experiment with a semiconductor nanowire.

3.1 Observations of conductance quantization

The first experimental observations of conductance quantization occurred in two-dimensional electron gases (2DEGs) in semiconductor heterostructures [9, 10]. In such experiments, an electron gas is confined between layers of semiconducting materials. A gate with tunable width is placed upon this heterostructure, allowing the energy-dependent conductance to be measured. The Fermi wavelength of 2DEGs is relatively large, typically around 40 nm, so that a gate width comparable to it can be experimentally realized. Such a gate is then called a quantum point contact.

Following these initial experimental results, conductance steps have been observed in several kinds of nanoscale systems. An important class of experiment is based on separating two electrodes, whereby a nanostructure known as a break junction is formed between them. Such break junctions are of very small dimensions, typically on the order of a single nanometer or smaller, and the contacts between electrodes and break junctions are therefore called atomic point contacts. Due to their small size, conductance steps have been possible to observe in metallic break junctions for metals with sub-nanometer Fermi wavelengths [11, 12]. In semiconductor materials, the Fermi wavelength is on the order of tens of nanometers and conductance steps have been observed in break junctions of larger size [13].

More recently, observations of conductance quantization have been reported for chemically synthesized nanowires in semiconductor materials [14, 15]. In these experiments, the nanowire width is on the order of tens of nanometers and length on the order of hundreds of nanometers. It is this type of nanowire, typically of Group III-V semiconductor material, that the present work focuses on.

3.2 Nanowires in semiconductor materials

In a typical electronic transport nanowire experiment a nanowire is attached to two metallic lead terminals called Source and Drain. An additional terminal is introduced, called the Gate terminal, which is close to, but not in contact with, the nanowire. Physically, this can be implemented in various ways. For example, the substrate on which the nanowire is fabricated (or a layer beneath it) can be used as gate terminal; this is known as a backgate. Increasing the gate voltage V_G corresponds to lowering the Fermi energy of the nanowire, changing the energy E of the system. The coupling between gate voltage and energy is called the lever arm $\alpha = E/eV_G$ of the system. The value of α, e.g. in meV per V, is usually not well known in an experimental setup; a lever arm prediction is one of the potential outcomes of transport simulations.

We mention a further experimental detail of the semiconductor nanowire experiments, namely that oscillations of Fabry-Pérot type have been observed in the energy-dependence of the nanowire conductance [16]. Such oscillations can be viewed as resulting from effective potential barriers at the lead-nanowire junctions. In this text, we do not discuss what exact physical mechanism the formation of such barriers may be attributed to.

Section 4

Numerical tight-binding model of transport

We now describe a method of computing the transport properties described in Section 2. In particular, we wish to compute the S-matrix for a nanowire with an arbitrary geometry, taking into account various effect as outlined in this section. In summary, we model the system with a tight-binding Hamiltonian, use the open-source Kwant code [4] to solve the discretized Schrödinger equation and compute the S-matrix. Finally, we extract the transport properties from this S-matrix.

We note that our model is a simple conduction-band effective mass model based on discretizing the Schrödinger equation, enabling a numerical solution. In contrast, the model is not atomistic, and the finite elements in the discretization do not correspond to single atoms, ions or any other physical entity. Hence, the model is independent of the crystal structure, atomic orbitals and similar physical properties of the nanowire material.

4.1 Discretized Schrödinger equation

We start by writing down a finite-difference discretized version of the Hamiltonian in (16), which is known as a tight-binding Hamiltonian. For simplicity, we assume a uniform magnetic field $\vec{B}$ in the xy-plane as illustrated in Figure 2, with the direction of the field described by an angle θ. We thus have

$$\vec{B} = (B\cos(\theta),\, B\sin(\theta),\, 0)\ . \tag{20}$$

This magnetic field can be represented as a vector potential $\vec{A}$ as given by $\vec{B} = \nabla \times \vec{A}$ in a number of ways. Choosing e.g. the Coulomb gauge $\nabla \cdot A = 0$ we have $A_x = A_y = 0$ and

$$A_z = B\left(y\cos(\theta) - x\sin(\theta)\right)\ . \tag{21}$$

Note that inserting this $\vec{A}$ into the Hamiltonian in (16) gives us

$$H = \frac{1}{2m^*}\left(-\hbar^2\nabla^2 + 2i\hbar e\vec{A}\cdot\nabla + e^2\vec{A}^2\right) + V(x,y,z) \tag{22}$$

where the second and third term in parentheses conventionally are called the paramagnetic and diamagnetic term, respectively.

The del operator $\nabla = (\partial/\partial x,\, \partial/\partial y,\, \partial/\partial z)$ is discretized using symmetric definitions of the derivatives. The discretized differential operator in the x-dimension of first order is given by

$$\frac{\partial g(x,y,z)}{\partial x} = \frac{g(x+a,y,z) - g(x-a,y,z)}{2a} \tag{23}$$

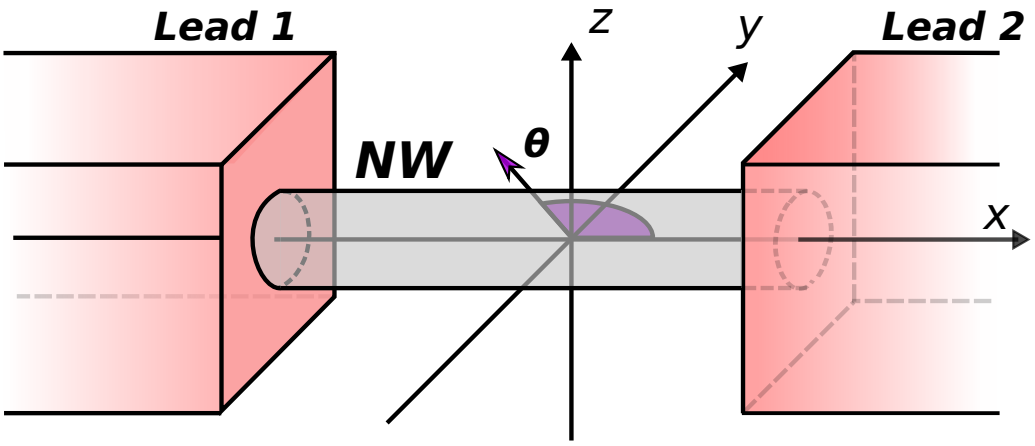

Figure 2: *A three-dimensional system with a nanowire (NW) placed between two leads. The angle θ describes the direction of a uniform magnetic field in the xy-plane.*

and of second-order by

$$\frac{\partial^2 g(x,y,z)}{\partial x^2} = \frac{g(x+a,y,z) - 2g(x,y,z) + g(x-a,y,z)}{a^2} \ . \tag{24}$$

where g is a test function and a is a finite number which can be made arbitrarily small. The expressions for the y- and z-dimensions are on the same form. Inserting these expressions into the Hamiltonian in (22), we obtain

$$\begin{aligned} Hg(x,y,z) = &\left(6\, g(x,y,z) - \sum_{NN} g(x,y,z)\right) t + \\ &+ \frac{i\hbar\omega_G}{2}\left(\frac{y}{a}\cos(\theta) - \frac{x}{a}\sin(\theta)\right)\left(g(x,y,z+a) - g(x,y,z-a)\right) + \\ &+ \frac{(\omega_G\hbar)^2}{4t}\left(\frac{y}{a}\cos(\theta) - \frac{x}{a}\sin(\theta)\right)^2 g(x,y,z) + V(x,y,z)g(x,y,z) \end{aligned} \tag{25}$$

where $g(x,y,z)$ is a test function, we have defined $t = \hbar^2/2m^*a^2$, introduced for convenience the gyrofrequency $\omega_G = eB/m^*$ and the nearest neighbor sum is given by

$$\begin{aligned} \sum_{NN} g(x,y,z) = &\, g(x-a,y,z) + g(x+a,y,z) + g(x,y-a,z) + g(x,y+a,z) + \\ &+ g(x,y,z-a) + g(x,y,z+a) \ . \end{aligned} \tag{26}$$

In (25) we have now written down a discretized version of the Hamiltonian in (16), which is suitable for numerical solutions.

4.2 Gaussian disorder potential

Real nanostructures inevitably exhibit disorder in the form of crystal imperfections, resulting e.g. from the fabrication process. This disorder is a fundamental source of

non-ballistic transport. We include disorder in our model using a Gaussian Disorder Model (GDM), where the potential $V(x, y, z)$ in (25) is pseudorandomly drawn from a Gaussian distribution centered at zero, with a distribution spread s_G corresponding to the disorder strength.

4.3 The Kwant code

In order to compute the transport properties we use the open-source Kwant code [4]. This software package was made available recently and is written mainly in the Python programming language. It provides a user-friendly way to input a discretized Hamiltonian, like the one in (25), and design a geometry, whereupon it uses numerical methods to solve the Schrödinger equation and compute various transport quantities, including the S-matrix. In this text, we will not discuss the mathematical methods employed by Kwant; for a description of these see Ref. [4].

4.4 Simulation procedure

As mentioned previously, the 3D grid which the spatial discretization corresponds to can be made arbitrarily dense, approaching the continuum limit for $a \to 0$. For all simulations we make a decision of the tight-binding resolution R in units of sites per nanometer, nm^{-1}, indicating the precision of the simulation. A criterion for well-resolved simulations is that

$$R\lambda_F >> 1 \ , \tag{27}$$

where λ_F is the Fermi wavelength of the system one wishes to model. As discussed in Section 3, λ_F is typically on the order of 10 nm for semiconductor materials. Therefore, we will usually pick R on the order of 1 nm^{-1} to fulfill the requirement in (27). After a resolution R has been selected, a physical dimension d should be represented by a number $N = Rd$ of discrete ‘‘sites’’ in the tight-binding simulation.

Computationally, it is convenient to make the assignment $t = 1$, for example because of machine precision limitations. This assignment results in an energy unit E_0 given by

$$E_0 = \frac{\hbar^2 R^2}{2m^*} \ . \tag{28}$$

A number of parameters with the dimension of energy, listed in Table 1, then have to be specified in units of E_0. The parameters τ and ϵ correspond to the temperature and finite Source-Drain bias as discussed in Sections 2 and 3.2. The strength of the uniform magnetic field described in Section 4.1 is controlled by η and the disorder discussed in Section 4.2 is controlled by σ.

Table 1: *List of numerical parameters used in the simulations.*

Symbol	**Parameter**	**Associated physics**
τ	$k_B T/E_0$	Temperature
ϵ	eV_{SD}/E_0	Source-Drain voltage
σ	s_G/E_0	Disorder
η	$\hbar\omega_G/E_0$	Magnetic field

Section 5

Results of simulations

In this section we present simulation results for a selection of systems, chosen in such a way as to demonstrate the versatility of our model.

5.1 Circular nanowire and its analytical solution

Here, we simulate fully ballistic circular nanowire in zero magnetic field and compute its conductance. We let $\tau \to 0$ and $\epsilon \to 0$. We take the nanowire to have a diameter $d = 30$ nm and use a resolution of $R = 1.2$ nm^{-1}. Note that since the conductor is fully ballistic its length does not, in this case, affect its transport properties and we arbitrarily set it to 60 nm.

The results of the conductance computation is compared to an analytical solution. The 2D Schrödinger equation can be solved for a cylindrical geometry with hard-wall boundary conditions, which is what the transversal part of the present nanowire represents. We do not go through the details of the solution here, but simply write down the well-known result for the energy levels

$$E_{n,k} = \frac{2\hbar^2}{m^* d^2} j_{n,k} \tag{29}$$

where $j_{n,k}$ is the kth zero of the Bessel function J_n. From Section 2.1 we know that each new transversal mode should represent an integer step of G_0 in the conductance, under the conditions in this simulation. These steps, as given by (29), we therefore call the analytical solution. The simulation result, together with the analytical solution, is shown in Figure 3. The discrepancy between the two curves that can be seen in this figure becomes smaller if the resolution of the simulation is increased.

5.2 Effects of temperature, Source-Drain bias, disorder and geometry

In these simulations we study how some of the physical effects we have described affects the nanowire conductance. We begin with the effects of temperature, Source-Drain bias and disorder; the first two have been introduced in Section 2 and the latter one in Section 4.2. For this, we use the same nanowire and resolution as in Section 5.1. In each simulation, we wish to isolate the effect we are concerned with, so we choose the parameters to diminish other effects. In all of these simulations we let $\eta = 0$. The results are presented in Figure 4.

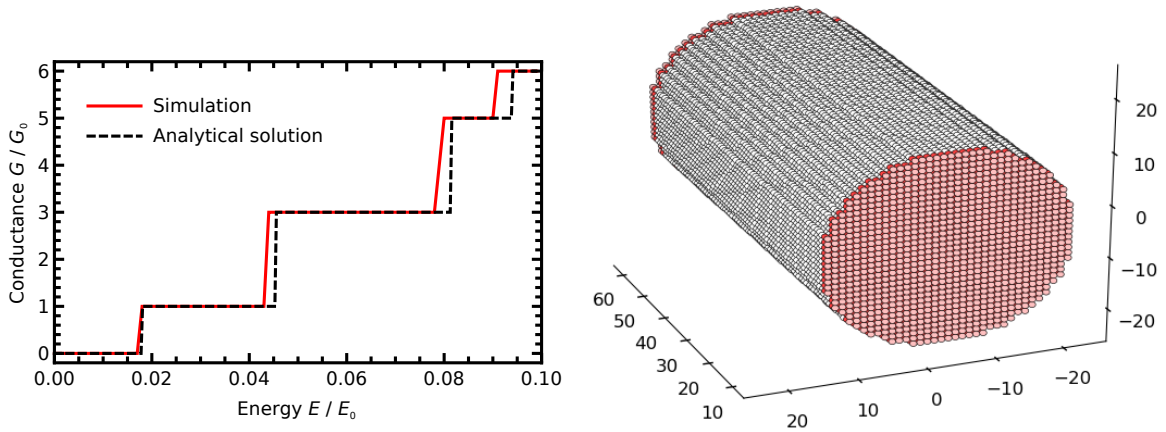

(a) (b)

Figure 3: (a) *Simulation results and comparison to analytical solution for the conductance of the circular nanowire described in Section* 5.1. (b) *A visualization of the tight-binding model of the nanowire produced by* Kwant. *Red regions represent semi-infinite leads.*

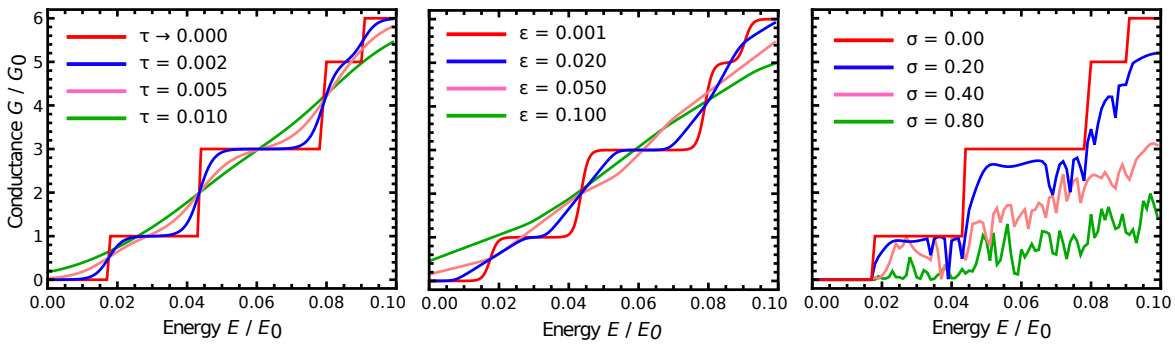

(a) (b) (c)

Figure 4: *Simulation results for the conductance of the nanowire described in* Section 5.1 *with different effects applied.* (a) *Effects of finite temperature with* $\epsilon \to 0$. (b) *Effects of finite Source-Drain bias; for all curves* $\tau = 0.001$. (c) *Effects of disorder; here* $\tau \to 0$ *and* $\epsilon \to 0$.

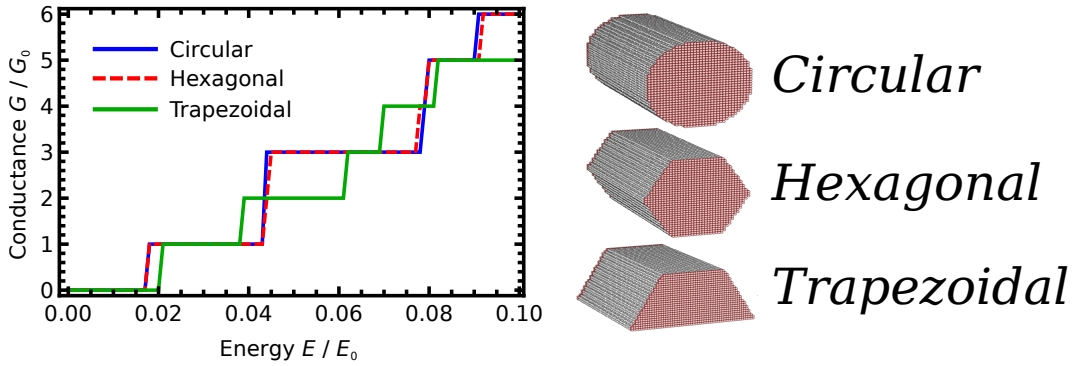

(a) (b)

Figure 5: (a) *The conductance of fully ballistic nanowires with three different transversal geometries, described in* Section 5.2. (b) *Models of the relevant nanowires visualized in* Kwant. *Red regions represent semi-infinite leads.*

Moreover, we study how the transversal geometry affects the conductance steps. In particular, we investigate whether some geometries break the degeneracy of the second and third step we observed for the circular geometry discussed in Section 5.1. In addition to the circular geometry, we simulate nanowires with a hexagonal and trapezoidal shape. We choose the dimensions of the nanowires such that their transversal areas are roughly the same. Using the same circular nanowire as before, this means that the hexagonal nanowire will have a flat-to-flat distance $d = 28.6$ nm. The trapezoidal geometry is achieved by truncating the hexagonal one and will hence correspond to a $d = 40.4$ nm hexagonal nanowire cut in half. We let $\eta = 0$, $\tau \to 0$ and $\epsilon \to 0$. A comparison of the conductances of the different nanowires are presented in Figure 5.

5.3 Hexagonal nanowire in magnetic field

We now study the effects of the presence of a finite uniform magnetic field on the conductance of a fully ballistic hexagonal nanowire. The configuration of the magnetic field is precisely as described in Section 4.1. We choose to simulate a nanowire with a flat-to-flat distance of 30 nm and a length of 60 nm, and we use a resolution $R = 0.8$ nm^{-1}. We let $\tau \to 0$ and $\epsilon \to 0$. We consider three different angles in the interval $0 \leq \theta \leq \pi/2$ and control the B-field strength with the parameter η, choosing values so that the full range of the effect is qualitatively visible. The results are presented in Figure 6.

5.4 Fabry-Pérot resonances in a circular nanowire

As discussed in Section 3.2, Fabry-Pérot oscillations may occur in the conductance of nanowires, as a result of the properties of the lead-nanowire junctions. In these simulations, we wish to simulate this effect. We do so by adding a potential barrier of height V_G

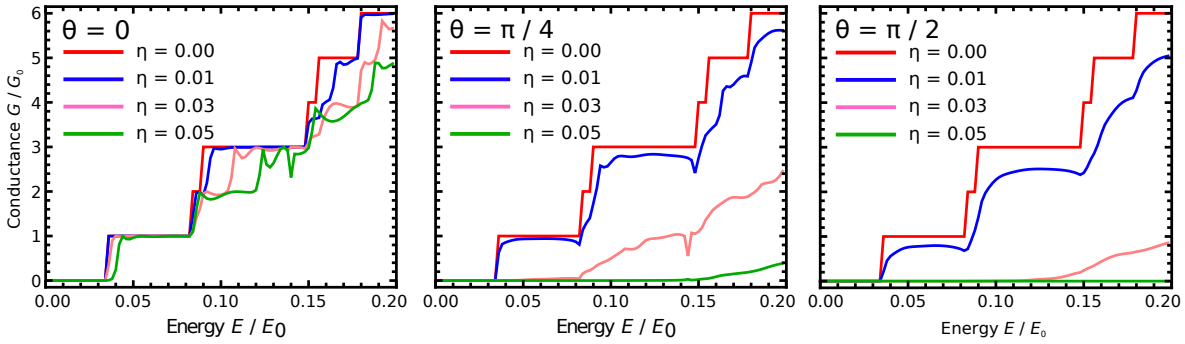

(a) (b) (c)

Figure 6: *Simulation of the effect of a uniform magnetic field on the conductance of a fully ballistic hexagonal nanowire. The details of the nanowire is described in* Section 5.3. *The direction of the magnetic field is controlled by the angle* θ *as in* Figure 2 *and the magnitude by the parameter* η *defined in* Table 1. *The figures* (a), (b) *and* (c) *show the results for three different angles, where* $\theta = 0$ *is parallel to the propagating direction and* $\theta = \pi/2$ *is perpendicular to it.*

near each lead in the nanowire; such a double barrier is quantum mechanically associated with Fabry-Pérot resonances. We simulate the conduction with Fabry-Pérot resonances in a system with equal dimensions and resolution as the circular nanowire described in Section 5.1. Again we let $\eta = 0$, $\tau \to 0$ and $\epsilon \to 0$. In addition, we perform the same simulation with a nanowire of double length (120 nm) to illustrate the length-dependence of the Fabry-Pérot oscillations. The results are presented in Figure 7.

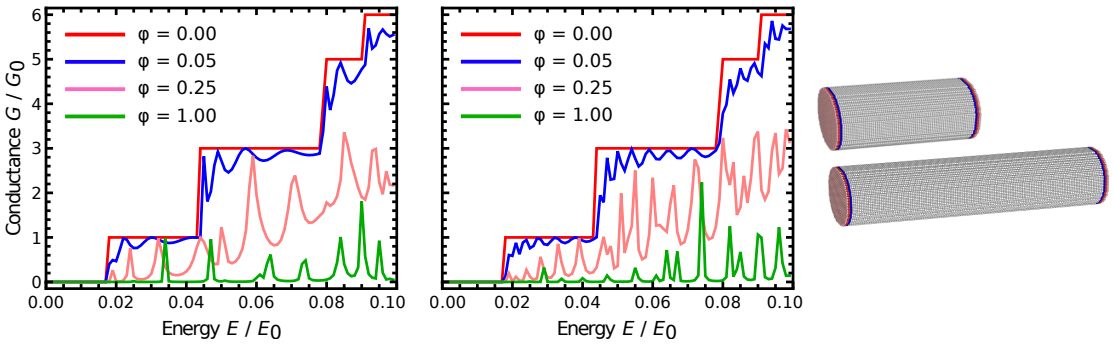

(a) (b) (c)

Figure 7: *Fabry-Pérot resonances in the conductance of two circular nanowires of different lengths. The potential barrier height V_B is controlled by the $\phi = V_B/E_0$ parameter.* (a) *Simulation of conductance in the nanowire described in* Section 5.1. (b) *Simulation with a nanowire twice the length of the former* (120 nm). (c) *Visualizations of the two nanowire models produced with* Kwant. *Blue regions represent potential barriers with height V_B and red regions represent semi-infinite leads.*

Section 6
Discussion and outlook

In Section 5 we have seen several results for how a number of physical conditions affect the electronic transport properties of semiconductor nanowires. We have demonstrated the ease of which different systems can be described using the tight-binding model outlined in Section 4. In the simulations, we have made use of the parameters listed in Table 1; in principle, the numerical values we have set these parameters to indicate in what energy regimes the effects should become significant.

Discussions of the individual simulations now follows. In Section 5.1 we saw how the simulation results could be matched with an analytical solution for the simple case of a fully ballistic cylindrical nanowire. The correlation with the analytical solution indicates that the numerical simulations are accurate. As energy increases, a small discrepancy can be observed. The source of this discrepancy can be presumed to be related to the criterion in (27), and does indeed decrease in simulations with higher resolutions.

The basic way in which temperature, finite Source-Drain bias, disorder and geometry affects the conductance steps were presented in Section 5.2. Temperature and Source-Drain bias ''smears'' the steps, in both cases approaching curves where plateaus in the curve are no longer distinguishable for large values of the associated parameters. The disorder included using the model described in Section 4.2 resulted in a suppression of conductance and a generally more ''noisy'' conductance curve. We note two things in particular. Firstly, disorder in combination with temperature or finite Source-Drain bias (all three of which are always present to some degree experimentally) can from the simulation results be understood to result in a smooth but modified conduction curve. This might offer a simple explanation of experimental observations of non-ideal steps. Second, we note that for low levels of disorder (see the $\sigma = 0.20$ curve in Figure 4) the deviations from the ideal conductance step are concentrated at the end of each individual step. This effect is indeed reproducible within the model, i.e. the result did not occur only for a single pseudorandomly generated disorder potential. Further investigation of this effect, including attributing it to a physical mechanism, is of interest to future research, since it corresponds to a clear signature in the conduction curve.

Keeping the transversal area of the nanowire constant, we saw also in Section 5.2 that we obtained the same result for the conductance of a cylindrical and hexagonal nanowire, which is a somewhat nontrivial result. Truncating the hexagonal shape into a trapezoidal one, we saw that the degeneracy of the second and third steps was broken.

In the simulations in Section 5.3 we studied the effect on conductance of a uniform magnetic field for a hexagonal nanowire. We saw two distinct effects, the weighting between them depending on the direction of the B-field. For a B-field parallel to the propagating direction of current, an effect similar to degeneracy-breaking was observed.

When the direction of the B-field was perpendicular to the direction of current, the corners of the conductance steps were rounded and slightly suppressed. In the interpretation of these effects, we remind ourselves that the model is non-atomistic, so that no quantum mechanical treatment of spin-degeneracy breaking has been manually added. A careful interpretation of the results in Figure 6 taking this into account is a topic for further investigation.

When metallic Source and Drain contacts are attached to semiconductor nanowires the nature of these junctions typically affects the electronic transport properties of the system. In the simulations in Section 5.4, we saw how the way in which Fabry-Pérot oscillations resulted from effective potential barriers at the lead-nanowire junctions.

In conclusion, we have demonstrated the versatility of a tight-binding approach to modeling electronic transport in semiconductor nanowires. The model used together with the Kwant code [4] provides a toolset for numerical computation of the S-matrix in general and the conductance in particular, with the possibility of including a number of different physical effects in the simulations.

6.1 Outlook

The most clear step for future research in this topic is to use the model to attempt to reproduce experimental results. This type of research could potentially contribute to the understanding of experimental data, and highlight the origin of certain features in the experimentally measured nanowire conductance.

Furthermore, there are a number of ways in which the model could be expanded upon in further research. In Section 2.1 we made the assumption that the voltage drop occurs entirely in the lead-conductor junctions. In principle, however, the applied voltages at all (Source, Drain and Gate) terminals give rise to an electrostatic field within the nanowire. If we wanted to account for effects of this field in the model, the possibility of including a numerical solver of Poisson's equation in the simulations could be investigated.

Another possible direction for future research could be, after correlating simulation results with experimental data, to compare the present model with an atomistic model. In such a model, one could in principle take into account material parameters such as crystal structure and occupied electron orbitals.

Section 7

Acknowledgements

I would like to thank Peter Samuelsson for supervising the project and for always being helpful and inspiring. Discussions with fellow student Emil Johansson were helpful in getting started with Kwant. I would also like to thank the Division of Mathematical Physics, and the Department of Physics as a whole, at Lund University for providing a great environment in which to study and do research. Finally, I would like to thank the Kwant community; the Kwant mailing list has been a great learning resource throughout the course of the project.

Bibliography

[1] N. P. Dasgupta, J. Sun, C. Liu, S. Brittman, S. C. Andrews, J. Lim, H. Gao, R. Yan, and P. Yang, Advanced Materials **26**, 2137 (2014).

[2] R. Landauer, IBM Journal of Research and Development **1**, 223 (1957).

[3] R. Landauer, Z. Phys. B - Condensed Matter **68**, 217 (1987).

[4] C. W. Groth, M. Wimmer, A. R. Akhmerov, and X. Waintal, New J.Phys. **16**, 063065 (2014).

[5] M. Büttiker, Phys. Rev. Lett. **57**, 1761 (1986).

[6] S. Datta, *Electronic Transport in Mesoscopic Systems* (Cambridge University Press, Cambridge, 1995).

[7] P. N. Butcher, J. Phys.: Condens. Matter **2**, 4869 (1990).

[8] Y. M. Blanter and M. Büttiker, Phys. Rep. **336**, 1 (2000).

[9] B. J. van Wees, H. van Houten, C. W. J. Beenakker, J. G. Williamson, L. P. Kouwenhoven, D. van der Marel, and C. T. Foxon, Phys. Rev. Lett. **60**, 848 (1988).

[10] D. A. Wharam, T. J. Thornton, R. Newbury, M. Pepper, H. Ahmed, J. E. F. Frost, D. G. Hasko, D. C. Peacock, D. A. Ritchie, and G. A. C. Jones, J. Phys. C **21**, L209 (1988).

[11] J. I. Pascual, J. Méndez, J. Gómez-Herrero, A. M. Baró, N. Garcia, U. Landman, W. D. Luedtke, E. N. Bogachek, and H.-P. Cheng, Science **267**, 1793 (1995).

[12] C. J. Muller, J. M. van Ruitenbeek, and L. J. de Jongh, Phys. Rev. Lett. **69**, 140 (1992).

[13] J. L. Costa-Krämer, N. García, and H. Olin, Phys. Rev. Lett. **78**, 4990 (1997).

[14] I. van Weperen, S. R. Plissard, E. P. A. M. Bakkers, S. M. Frolov, and L. P. Kouwenhoven, Nano Lett. **13**, 387 (2013).

[15] S. Chuang, Q. Gao, R. Kapadia, A. C. Ford, J. Guo, and A. Javey, Nano Lett. **13**, 555 (2013).

[16] A. V. Kretinin, R. Popovitz-Biro, D. Mahalu, and H. Shtrikman, Nano Lett. **10**, 3439 (2010).